Physics of Plasmas

Filamentation of capacitively coupled plasmas in large magnetic fields EP

Cite as: Phys. Plasmas **26**, 063515 (2019); https://doi.org/10.1063/1.5092600
Submitted: 12 February 2019 . Accepted: 03 June 2019 . Published Online: 21 June 2019

Mohamad Menati, Edward Thomas, and Mark J. Kushner

AIP Publishing

Physics of Plasmas ARTICLE scitation.org/journal/php

Filamentation of capacitively coupled plasmas in large magnetic fields

Cite as: Phys. Plasmas **26**, 063515 (2019); doi: 10.1063/1.5092600
Submitted: 12 February 2019 · Accepted: 3 June 2019 ·
Published Online: 21 June 2019

Mohamad Menati,[1,a)] Edward Thomas,[1,a)] and Mark J. Kushner[2,b)]

AFFILIATIONS

[1]Department of Physics, Auburn University, Auburn, Alabama 36849-5311, USA
[2]Department of Electrical Engineering and Computer Science, University of Michigan, 1301 Beal Avenue, Ann Arbor, Michigan 48109-2122, USA

[a)]Electronic addresses: mzm0085@tigermail.auburn.edu and etjr@auburn.edu
[b)]Author to whom correspondence should be addressed: mjkush@umich.edu

ABSTRACT

Over the last decade, dusty plasma research has sought to explore the physics of magnetized dusty plasmas. Due to the small charge-to-mass ratio of micron-sized dust grains, magnetic fields of $B \geq 1$ T are needed to magnetize these particles. A peculiar phenomenon that occurs in capacitively coupled, glow discharge dusty plasmas at high magnetic fields that are perpendicular to the electrodes is the formation of stationary or mobile filamentary structures that are aligned along the magnetic field. In experiments, these filaments are found to form at a low neutral gas pressure, low applied radio frequency power, and a high magnetic field. This paper reports on new simulations of capacitively coupled plasmas at a high magnetic field for a configuration with a powered metal electrode and a grounded electrode with a dielectric barrier. It is shown that for this configuration, it is possible to form filamentary structures that appear in the electron density, potential, and light emission, which have properties that scale qualitatively with experiments. For these conditions, the dielectric strength of the boundary is most strongly correlated with the formation of the filaments. Implications of these observations and how they could be used to motivate future experiments are discussed.

I. INTRODUCTION

Dusty plasmas are unique platforms for the study of nonideal systems. Dusty plasmas in this context typically consist of low temperature, capacitively coupled plasmas (CCPs) which have been seeded with nonreactive dielectric particles, the dust, having diameters of a few to tens of microns.[1,2] In these systems, the particles naturally negatively charge to the electrical floating potential of the plasma and in doing so can contain a substantial portion of the negative charge in the plasma.[3,4] The resulting system is charge balanced, in large part, by mobile positive ions and immobile particles of far smaller number density each having $Z_d = 10^3$–10^4 negative charges.[5–7] The nonideality factor, also known as the Coulomb coupling parameter, for dusty plasmas is $\Gamma = Z_d q 2 N_d^{1/3}/T_d$, where N_d is the dust number density and T_d is the particle temperature, and is a measure of Coulombic potential energy compared to the random thermal energy of the system.[8] Γ can be tens to thousands, making dusty plasmas an ideal platform for investigating thermodynamic transitions,[9–12] soliton wave propagation,[13,14] and self-organization.[15–17]

Recent interest in dusty plasma physics has included investigating magnetized dusty plasmas (MDPs) in which an external magnetic field is applied to magnetize the electrons, ions, and, under the right conditions, the dust particles. In experiments in which micron-sized particles are used, their charge (~1000–5000 elementary charges)-to-mass (~10^{-14}–10^{-15} kg) ratio is quite small, thereby requiring magnetic fields of $B \geq 2$ T in order to magnetize the dust particles. A commonly used configuration for MDPs is a parallel plate CCP sustained in a rare gas such as argon having pressures of tens to hundreds of millitorr, at powers of a few to tens of watt with the external magnetic field applied perpendicular to the electrodes. In experiments at these high magnetic fields without added dust particles, these CCP plasmas are observed to form filaments parallel to the magnetic field and perpendicular to the electrodes.[18–20] The filaments, diagnosed by optical emission, bridge the interelectrode gap. The filaments are typically nonstationary and will often form patterns of dots, circles, and spirals.[19] The filaments are more likely to form at low gas pressures, low power deposition, and a high magnetic field.[21] The typical spacing of the filaments is a few millimeters having a width or diameter of 1–2 mm. The filaments appear to retain the integrity of their gap-crossing luminous structures while translating horizontally parallel to the electrodes. This motion may be oscillatory with a spatial period of up to a centimeter or moving many millimeters to a few centimeters, from one quasistationary position to another.

An experimental example of these filamentary structures is shown in Fig. 1. Here, the filaments are observed in visible light emission from an argon CCP plasma in the Magnetized Dusty Plasma Experiment (MDPX) device at Auburn University.[22,23] The filaments form between a powered, 30 cm diameter, lower electrode and a grounded, 30 cm diameter, upper electrode that has a 15 cm diameter hole that is covered by an indium-tin-oxide (ITO)-coated (i.e., conducting surface) glass plate. The filaments are viewed through a 25 cm diameter viewport at the top of the vacuum chamber. For this experiment, the neutral pressure was fixed at $p = 100$ mTorr and the magnetic field was $B = 1.0$ T. The applied radio frequency (RF) power is increasing in the figure: (a) 5 W, (b) 15 W, (c) 25 W, and (d) 40 W. At low power, individual filaments (near the center) and concentric circular structures are observed. With increasing power, the individual filaments and the circular structures appear to dissipate. This example is presented to illustrate the various structures that filaments can form in the MDPX device rather than showing a specific experimental case to that simulated. Filaments can be observed in the MDPX device in cases where there is one conducting electrode and one dielectric electrode and also when both electrodes are conducting (as illustrated here) although the electrodes likely have dielectric contamination.

In this paper, the origins of plasma filaments in low pressure, argon CCPs are discussed using the results from a computational investigation. The goal of this work is to offer new insights into a particular experimental configuration that could lead to the formation of filaments and to motivate continuous experimental studies. Although the motivation of this work is in the use of magnetized CCPs in the study of dusty plasmas, cross-magnetic field transport is also an important phenomenon in many applications of low temperature plasmas, such as magnetrons[24] and Hall effect thrusters.[25] In this work, we have found that the filaments are quasistationary structures that originate from statistical variations in the local plasma potential and charging of surfaces. There is a tendency toward self-organization where filaments are evenly spaced although these spacings are also somewhat statistical. Consistent with the experimental observations by Schwabe *et al.* (reported in terms of a magnetization strength, χ),[19] the filaments dissipate as $\chi = \frac{\lambda_{mfp}}{\rho_{ion}} = \frac{\textit{ion mean free path}}{\textit{ion gyroradius}} \sim \frac{B}{N}$ (i.e., strength of the magnetic field/gas number density) decreases. In these simulations (gas pressure 40 mTorr), the onset of filaments occurred at $B = 100$–500 G. For $B = 1000$ G, the filaments began dissipating in the simulations for pressures exceeding 250–300 mTorr.

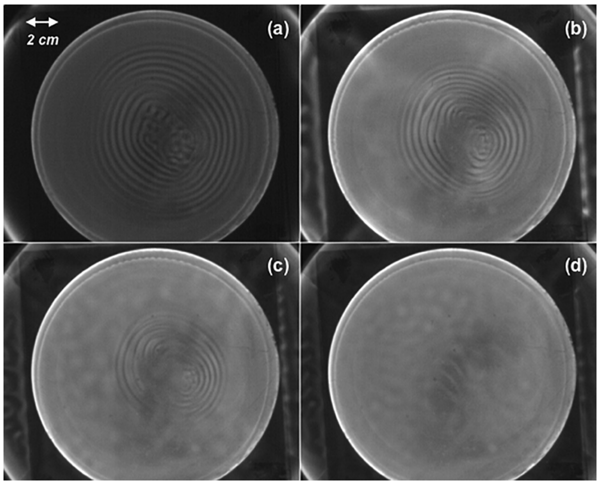

FIG. 1. Filaments observed in visible light in an argon CCP plasma in the MDPX device. The filaments are viewed through an indium-tin-oxide coated glass plate embedded in the top electrode. The gray "spots" and spiral structures are the filaments that are formed in the plasma. The neutral pressure was $p = 100$ mTorr, and the magnetic field was $B = 1.0$ T. The applied RF power increases from (a) 5 W, (b) 15 W, (c) 25 W, and (d) 40 W. At a low power, individual filaments (near the center) and concentric circular structures are observed.

The configuration of the CCP investigated here was a metal powered electrode and a grounded metal electrode placed behind a dielectric window. The strongest correlation of filaments with operating conditions was the surface conductivity of the dielectric window. In these simulations, filaments did not form if the ground electrode opposite the powered electrode was directly exposed to the plasma or if the dielectric had significant surface conductivity. With the grounded electrode covered by the dielectric window, filaments formed due to stochastic charging of the window.

II. DESCRIPTION OF THE MODEL

The simulation used in this investigation is the Hybrid Plasma Equipment Model (HPEM), described in detail in Ref. 26. The implementation of the HPEM with an externally applied magnetic field is described in Ref. 27. In summary, the continuity, momentum, and energy equations for ions, neutral particles, and electrons are solved on a 2-dimensional Cartesian mesh. Tensor forms of transport coefficients are implemented with an effective collision frequency for electrons to account for anomalous cross-magnetic field transport. The effective collision frequency is chosen to be the larger of the actual momentum transfer collision frequency or $0.003\omega_c$, where ω_c is the cyclotron frequency, a semiempirical relationship derived from simulations of magnetron sputtering and MERIE (magnetically enhanced reactive ion etching) discharges.[28,29] Charge accumulation on nonmetal surfaces is computed based on the fluxes of incident electrons and ions, secondary electron emission, and conduction through the solid. The resulting charge densities on and in the solids, in addition to the charge densities in the plasma, are then used in the solution of Poisson's equation for the electric potential. The working gas is argon. The reaction mechanism used in the model is the same as that presented in Ref. 30, including species Ar, Ar($1s_2$), Ar($1s_3$), Ar($1s_4$), Ar($1s_5$), Ar(4p), Ar(4d), Ar^+, and electrons.

The method for computing the Jacobian elements in solving the matrix for Poisson's equation in the model is different depending on whether you have a 5-point numerical molecule ($B = 0$) or a 9-point numerical molecule ($B > 0$). To ensure that the same algorithms are used in all cases and to minimize any possible systematic error, we used $B = 10^{-10}$ G instead of $B = 0$. That is, computational results for $B = 0$ actually used $B = 10^{-10}$ G. We confirmed that using $B = 10^{-10}$ G and $B = 0$ provides essentially the same answer, but chose to error on the side of caution by using the finite value.

The geometry used in this investigation, shown in Fig. 2(a), is intended to be a generic CCP that is inspired by the spatial dimensions and configurations of the MDPX device where either the top or bottom electrode can be powered. The configuration described in

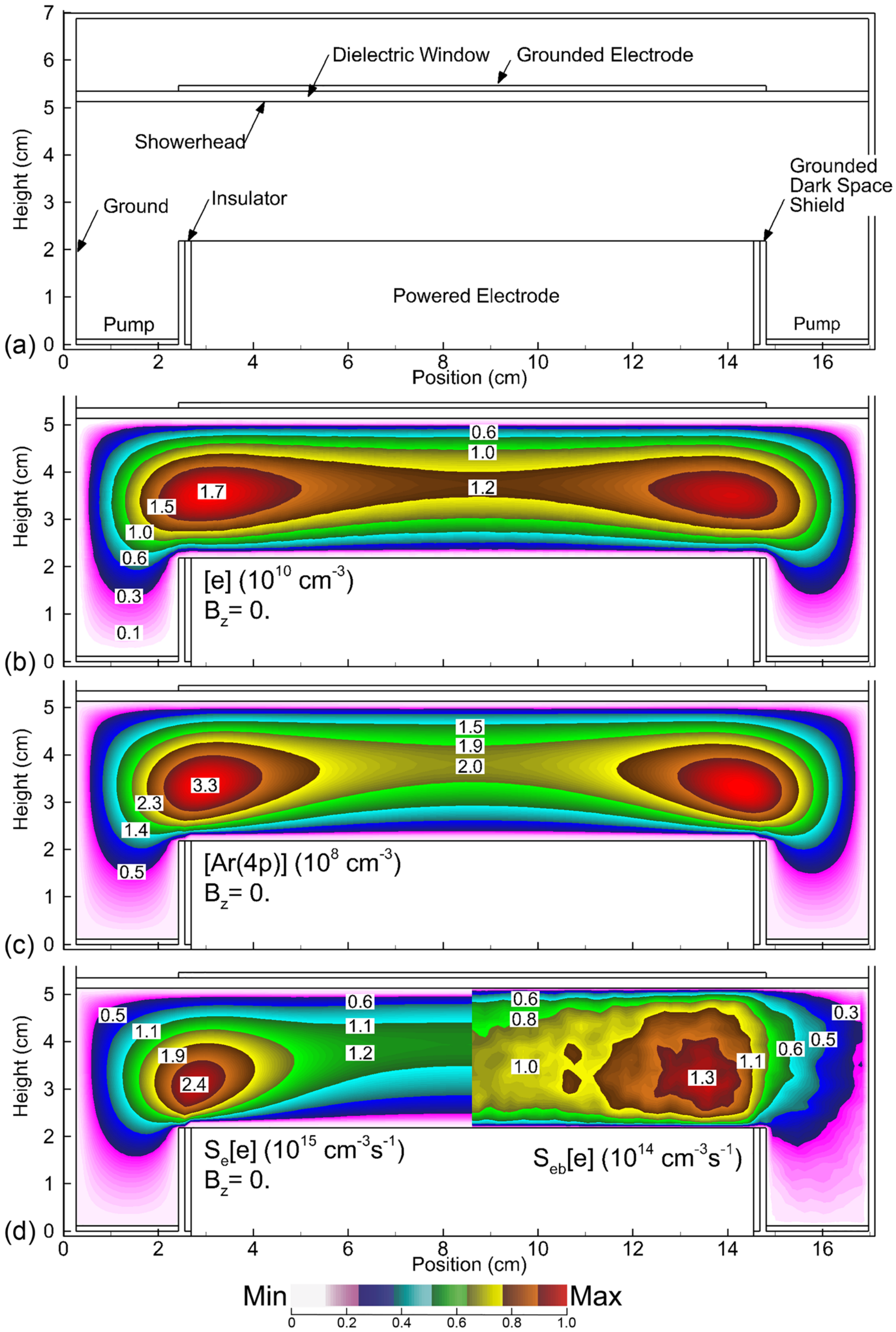

FIG. 2. Reactor conditions and unmagnetized plasma properties. (a) Geometry used for the simulation of the CCP. A 12 cm diameter powered bare metal electrode is surrounded on its outer diameter by a grounded dark space shield. The opposite grounded electrode sets on top of a 0.5 cm thick dielectric window with a dielectric constant of $\varepsilon/\varepsilon_0 = 4.0$. The plasma height is 3 cm. The applied magnetic field is uniform and purely in the axial direction perpendicular to the electrodes. The results of the unmagnetized ($B_z = 10^{-10}$ G) base case simulation of an argon CCP at $p = 40$ mTorr, an inlet flow rate of 300 sccm, and an applied voltage amplitude of 75 V at 10 MHz are shown. In the absence of a magnetic field, calculations of the (b) electron density, (c) density of the Ar(4p) state, which is the surrogate for optical emission, and (d) ionization sources for electrons through (left) collisions with bulk electrons and (right) sheath accelerated secondary electrons are shown. Images are plotted on a linear scale. Contour labels are multipliers for the base value shown in each image.

Fig. 2(a) is qualitatively similar to a MDPX configuration that was recently reported in a paper by Hall *et al.*[31] In the simulation, a 12 cm diameter powered bare metal electrode is surrounded on its outer diameter by a grounded dark space shield. The opposite grounded electrode sets on top of a 0.5 cm thick dielectric window with a dielectric constant of $\varepsilon/\varepsilon_0 = 4.0$. The surface conductivity of the dielectric will be varied. The secondary electron emission coefficient by ion bombardment was 0.15 for the electrode surface, 0.05 for the top dielectric, and 0.02 for the outer walls and dark space shield. The trajectories of secondary electrons are tracked using a kinetic Monte

Carlo simulation. The plasma height is 3 cm. The top window also serves as a gas showerhead, while gas is pumped on either side of the powered electrode. The applied magnetic field is uniform and purely in the axial direction perpendicular to the electrodes. The Cartesian mesh has a resolution of 1.1 or 0.67 mm in the lateral direction (perpendicular to the magnetic field) and 1.1 mm in the axial direction (parallel to the magnetic field). This resolution moderately resolves the axial sheath (a few mesh points). No significant changes were observed when using the higher resolution in test cases. The current resulting from the bias voltage applied to the substrate flows through a blocking capacitor upon which a dc bias forms. The amplitude of the applied voltage was held constant unless noted otherwise.

III. SCALING OF FILAMENTATION IN MAGNETIZED CCPS

In these simulations, the base case conditions have argon at 40 mTorr with an inlet flow rate of 300 sccm and an applied voltage amplitude of 75 V at 10 MHz. The plasma properties in the absence of a magnetic field are shown in Figs. 2(b)–2(d). (Unless noted otherwise, all the computed results are averaged over 1 RF cycle.) The electron density, shown in Fig. 2(b), though not uniform, is smooth without filaments or filamentation having a maximum value of $1.7 \times 10^{10}\ \mathrm{cm}^{-3}$. The peaking of the plasma density at the edge of the electrodes is a common occurrence in CCPs sustained in Ar, resulting from electric field enhancement at the edge of the electrode. No attempt was made to make the plasma more uniform. As a surrogate of the optical emission observed experimentally, the density of the Ar(4p) manifold is shown in Fig. 2(c). The density of Ar(4p) is also smooth, reflecting the distribution of electron density. The ionization sources for electrons through (left) collisions with bulk electrons and (right) sheath accelerated secondary electrons are shown in Fig. 2(d). The maximum local value of ionization by secondary electrons is about 5% that by bulk electrons (electron temperature 4 eV), but throughout the simulation volume, the secondary electrons contribute to about 10% of total ionization. The dc bias on the blocking capacitor is −20.1 V, resulting from asymmetries in the vacuum chamber.

The plasma facing surface of the dielectric charges negatively to $-7 \times 10^{-10}\ \mathrm{C/cm}^3$ at the center of the plasma. A dielectric in contact with the plasma will typically acquire surface charge that raises its potential to the floating electrical potential. The floating potential is a function of the electron and ion fluxes, and electron and ion temperatures. Since these values are not uniform across the face of the dielectric, the charge density on the surface of the dielectric is also not uniform. However, the variation of charge density across the face of the dielectric is smooth and continuous without stochastic noise.

While holding all the other initial conditions fixed, the electron and Ar(4p) densities and electron impact ionization sources are shown in Fig. 3 for an axial magnetic field of $B_z = 3500$ G (0.35 T). The plasma properties are now clearly striated or filamented. The electron temperature is nearly constant at 4.4 eV throughout the bulk plasma, with some stochastic variation between or on filaments of less than 0.1 eV. However, apart from the presence of the filamentary structures, the spatial distribution of the plasma is aligned with the metal biased electrode. Both sources of ionization, stochastic heating by bulk electrons and secondary electrons, originate from the essentially 1-dimensional sheath at the powered electrode. Since the electrons are magnetized and largely confined to the axial magnetic field lines, there is little lateral electron transport to convect electron energy beyond the edge of the electrodes. Computationally, if plasma is initially placed outside the boundaries of the powered electron, the plasma is not self-sustained and will decay away. The strong electron magnetization may also be contributing to the reduced effectiveness of the secondary electrons. In the absence of the magnetic field, electron scattering of sheath accelerated high energy secondary electrons enables ionization collisions beyond the confines of the electrodes. With magnetization along the vertical axis, scattering events are effectively either forward or backward.

The filaments in electron density are not terribly severe, having a variation of only a few percent. The Ar(4p) density, which is the surrogate for optical emission, is also striated with a larger modulation of 5%–10%. The modulation of the filaments of electron impact ionization is larger and more random than that of the densities, having an amplitude of 10%–15%. (The values of modulation were calculated by the difference between the local maximum and minimum, divided by the average extending over the range of several filaments.)

For the average electron temperature of about 4.4 eV, the gyroradius of electrons is about 0.02 mm, which is not resolved by the numerical mesh in the fluid portion of the simulation (even with the finer meshes used). The electron Monte Carlo simulation which tracks the trajectories of secondary electrons does resolve the gyroradius. It is true that filaments will at best be resolved on the resolution of the mesh, and we may be missing phenomena that are submesh on the spatial scale. However, when using finer meshes, the filaments did not shrink in width and experiments actually show filament widths that are somewhat larger than that predicted here. Although there may be mesh effects in the simulations, we do not believe that these effects dominate.

Although not shown in the figures, another output of the HPEM code is the charge density, which is a sum of densities of electrons, ions, and surface charge. We use this output to estimate the distribution of charging at several locations in the simulation. The charging of the top dielectric also shows some randomness, almost noise, although the average is essentially uniform. The magnitude of (negative) charging is about three times that in the absence of the magnetic field. The charge density at the middle of the gap without the magnetic field is essentially uniform and positive at $3.75 \times 10^{-13}\ \mathrm{C/cm}^3$ or the equivalent ion density of $2.3 \times 10^6/\mathrm{cm}^3$. This small amount of positive charge is responsible for generation of the confining ambipolar electric field, as should be the case for an electropositive plasma with a near uniform electron temperature. With a magnetic field, the charge density is striated or filamented with both positive- and negative domains with amplitudes as large as $\pm 2.5 \times 10^{-12}\ \mathrm{C/cm}^3$ or an equivalent ion density of $1.6 \times 10^7\ \mathrm{cm}^{-3}$. These filaments of charge densities then translate into perturbations in the plasma potential.

Although the sheaths at both the powered and dielectric surfaces remain essentially 1-dimentional during the RF cycle, the lateral variations of charge density on the filaments and on the dielectric surface do introduce a minor 2-dimensional structure into the sheaths. The general sequence is that stochastic charging of the dielectric coupled with the RF oscillation of the sheath launch electrostatic waves (positive and negative) that travel along the magnetic field lines and intersect the powered sheath. This charge density then modulates the width of the powered sheath, a variation that is at most a few percent at the peak of the cathodic cycle.

The transition from smooth to striated discharges is shown in Figs. 4 and 5, with images of Ar(4p) density (surrogate for optical

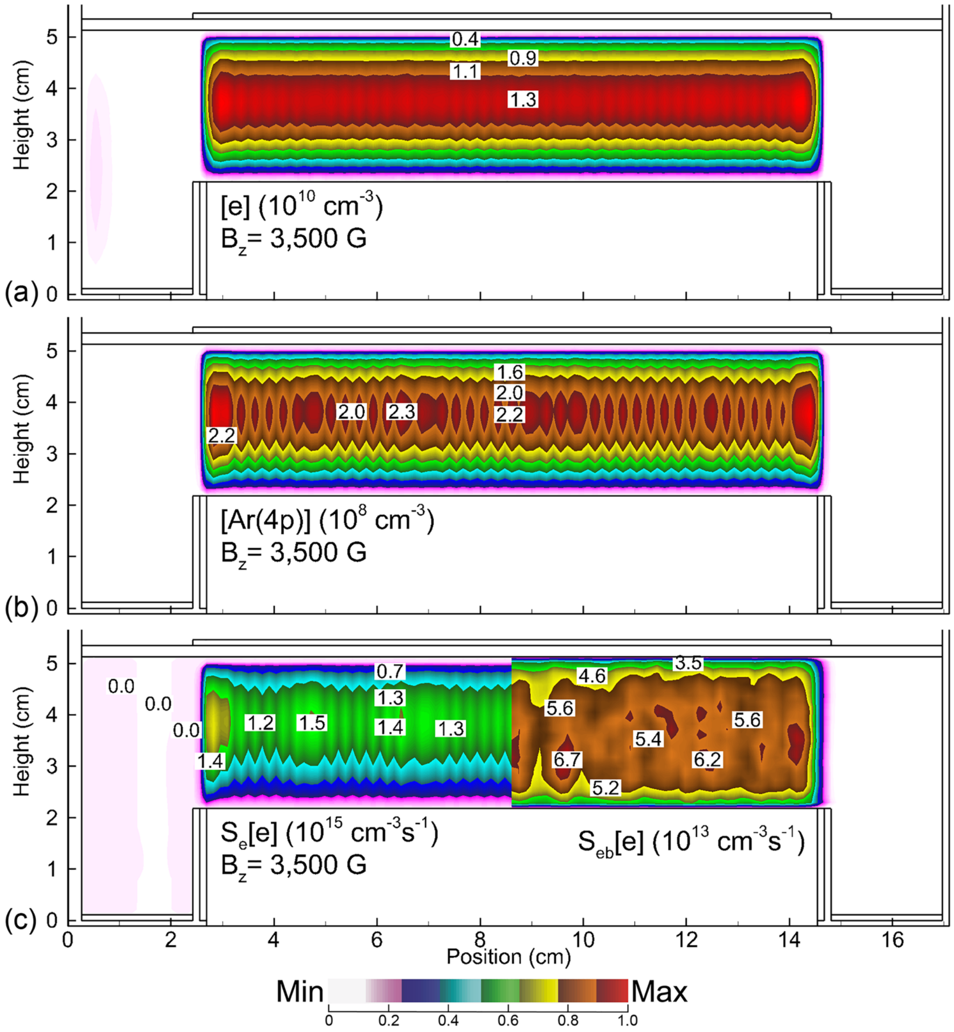

FIG. 3. Results of the simulation for the (a) electron density, (b) density of the Ar(4p) state, and (c) ionization sources for electrons through (left) collisions with bulk electrons and (right) sheath accelerated secondary electrons for the same conditions as Fig. 2, but with a magnetic field of B = 3500 G (0.35 T). Note the appearance of filamentary structures with a 5%–10% spatial variation in both the electron and Ar(4p) state (e.g., effective light intensity) densities. The images are plotted on a linear scale. Contour labels are multipliers for the base value shown in each image.

emission) and electron density for axial magnetic fields of $B_z = 0$–6000 G. The images are centered at the midgap and at a lateral position of 10 cm. Limited dynamic ranges (indicated in each frame) are plotted to emphasize the filaments. With $B_z = 0$, the densities of both electrons and Ar(4p) are smooth and increase to the right, reflecting the electric field enhancement at the edge of the electrode (to the right of the image). At $B_z = 100$ G, there is already modulation in densities and a transition to the laterally more uniform plasma produced by the axial magnetic field. By $B_z = 500$ G, filaments have formed, with their relative modulation amplitude increasing with the increasing axial magnetic field. Arguably, the Ar(4p) density is more striated than the electron density. In spite of Ar(4p) being able to freely diffuse across the magnetic field lines, its radiative lifetime is fairly short (0.1 μs), and so its density largely reflects the location where the atom was excited. In some ways, Ar(4p) is axially less mobile than electrons whose transport along the magnetic field is nearly unconstrained.

The filaments shown here are not stationary, having both ordered and random variations on a RF cycle-to-cycle basis. For example, the electron density is shown in Fig. 6 at the midgap (the same location as in Fig. 5), averaged over 1 RF cycle (0.1 μs), as a series of images separated by 25 RF cycles (2.5 μs). The experimentally observed motion of filaments occurs on the order of 0.1–1 s, longer time scales than that addressed here. Filaments in the simulations grow and decay on time scales of 5–10 μs although there are longer lived structures. It remains to be determined if these short-lived filamentary structures are responsible for the long-lived structures that are observed in the experiments. Moreover, these simulations suggest that measurements of laboratory filaments may need to take place with a substantially finer time resolution in order to determine the complete temporal evolution of these structures.

Computational tests were conducted to determine the sources of the filaments. In this model, the secondary electron emission is addressed using a Monte Carlo simulation that has inherent statistical noise, which could be the source of random perturbations that are trapped on magnetic field lines. When removing secondary emission processes, the filaments persisted. Although there are certainly almost unavoidable mesh effects, calculations were done with twice and three times the mesh resolution, and the filaments persisted. The electrode gap was increased by a factor of 1.5. Although the filaments weakened, they persisted, giving some indication that the sources of filaments are

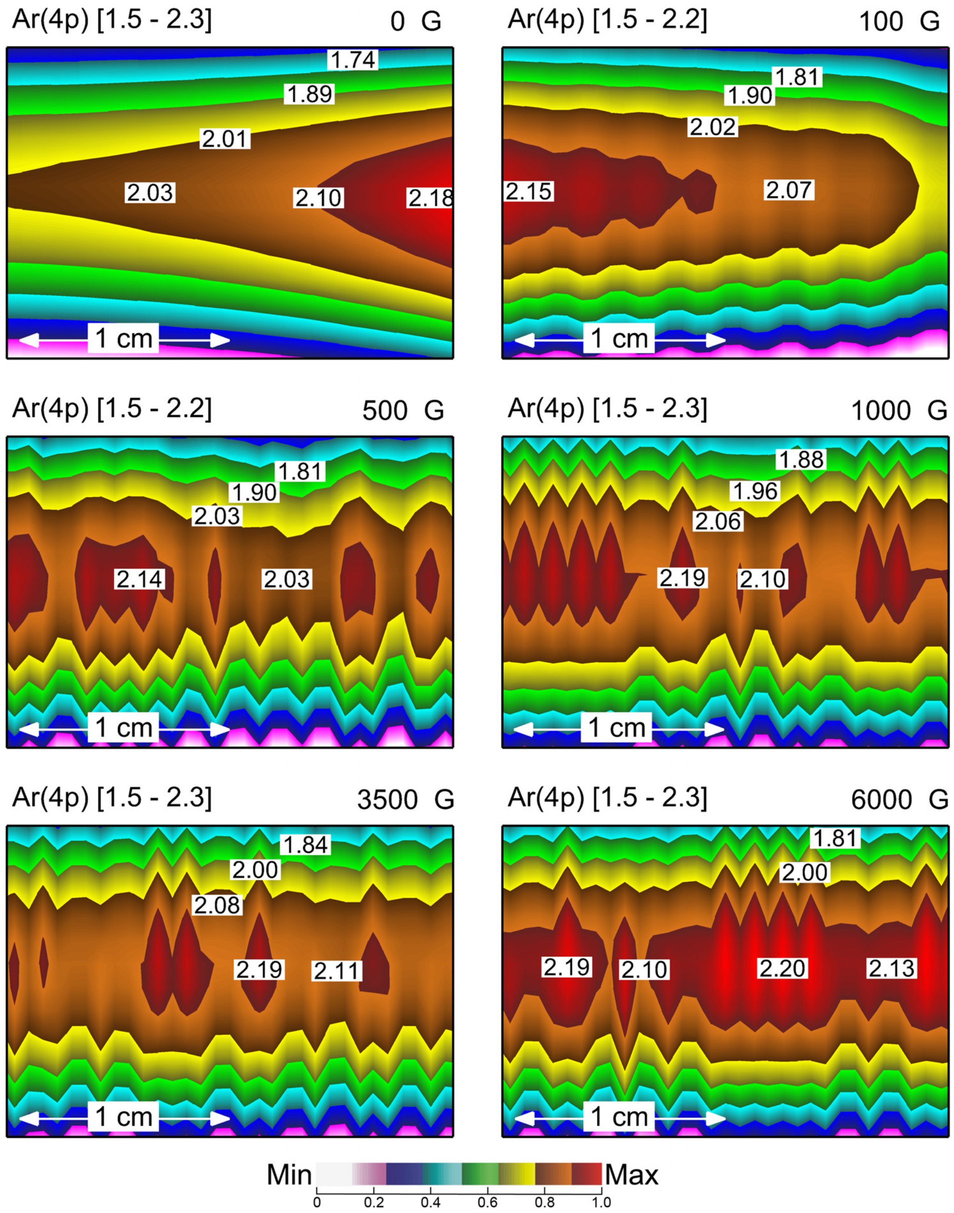

FIG. 4. The transition from smooth to striated discharges with an image of the Ar(4p) density (surrogate for optical emission) for axial magnetic fields from $B_z = 0$ to 6000 G. The images are centered at the midgap, $y \sim 3.5$ cm, and at a lateral position of $x = 10$ cm. The images show relative values over a limited range (indicated in each image) to emphasize the filaments.

associated with boundaries. Finally, calculations were performed for pressures from 20 mTorr to 400 mTorr. Again, the filaments weakened with increasing pressure but persisted, which might be expected as ν_m/ω_c increased and the electrons become less magnetized. As the pressure increases, the plasma density progressively reverts to the shape with $B_z = 0$ shown in Fig. 2, with a higher plasma density at a larger radius. At 250 mTorr, the filaments are essentially dissipated in the high plasma density regions where local power deposition (watt per cubic centimeter) is higher, while still persisting in the low plasma density region (lower watt per cubic centimeter). Computational experiments were performed for varying voltage and power. The effects of decreasing the filamentation with the increasing electrode gap, increasing pressure, or increasing power density are generally consistent with the experimental observations that have been made in the MDPX device.

Other than increasing pressure to the point that the plasma is no longer magnetized or moving the top surface to such a large distance that plasma barely touched it, the operational condition that most affects the formation of the filaments in the simulation is the conductivity of the plasma facing dielectric. Electron densities for $B_z = 3500$ G as a function of the surface or sheet conductivity of the plasma facing dielectric are shown in Fig. 7. Numerically, the surface or sheet conductivity of the dielectric was represented by enabling conductivity only between the mesh points on the surface of the top dielectric in contact with the plasma. This sheet conductivity might occur as a result of UV or vacuum-UV emission from the plasma producing

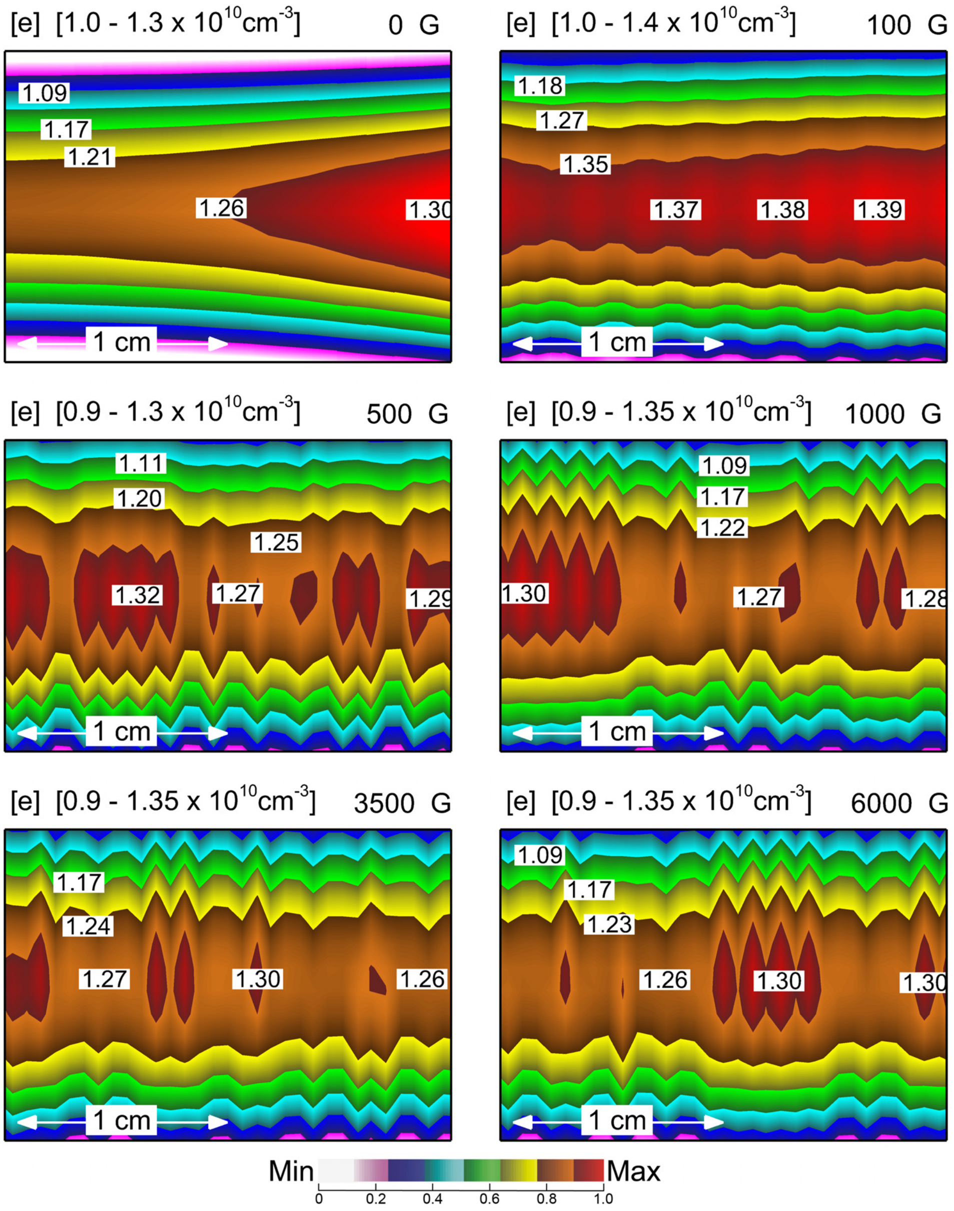

FIG. 5. The transition from smooth to striated discharges with an image of the electron density for axial magnetic fields from $B_z = 0$ to 6000 G. The images are centered at the midgap, $y \sim 3.5$ cm, and at a lateral position of $x = 10$ cm. A limited range of values (indicated in each image) is plotted to emphasize the filaments.

mild photoconductivity, ion bombardment, or mobility of physisorbed charge species.[32,33] The default conductivity of the dielectric is $\sigma = 10^{-10}/\Omega$ cm.

With the sheet conductivity of $\sigma_S = 10^{-10}/\Omega$ cm, the filaments appear identical to that of the base case—albeit with differences attributable to statistical noise. Increasing the sheet conductivity to $\sigma_S = 10^{-5}/\Omega$ cm had little effect on the filaments, other than statistical variation. When progressively increasing σ_S to $10^{-4}/\Omega$ cm and higher, the filaments began to dissipate. With $\sigma_S = 3 \times 10^{-5}/\Omega$ cm, the filaments are widely spaced with only slow spatial variation in time. For larger values of σ_S, the filaments fully dissipate, with the discharge closely resembling that of the metal top electrode.

IV. CONCLUDING REMARKS

Filaments are commonly observed in magnetized capacitively coupled plasmas of the type used in magnetized dusty plasma experiments. Operating conditions are typically rare gas plasmas sustained in a few centimeters gap, pressures of tens to hundreds of millitorr, and RF powers of a few to tens of watts. Externally applied magnetic fields of up to a few Tesla are applied perpendicular to the electrodes. A computational investigation was performed on a parallel plate CCP sustained in argon for conditions similar to those of dusty plasma experiments to determine the source of the filamentation. A critical feature of the simulation is that one electrode in the CCP is metal and the other electrode is a dielectric barrier covering a grounded electrode.

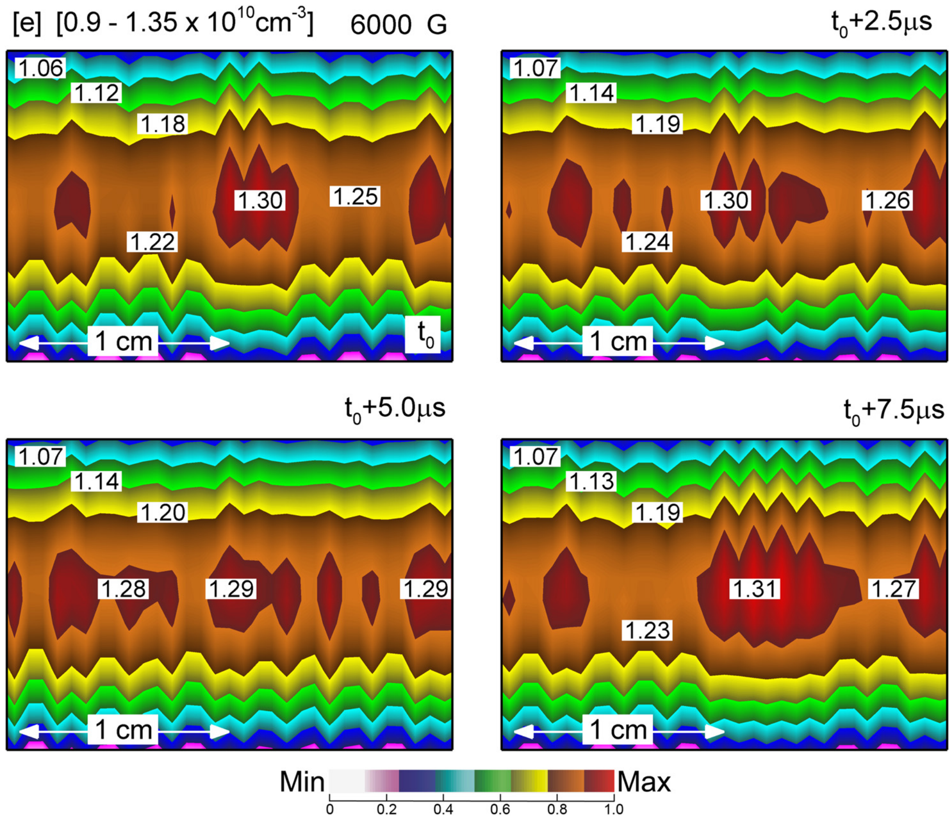

FIG. 6. The electron density at the midgap (the same location as in Figs. 4 and 5), averaged over 1 RF cycle (0.1 μs), as a series of images separated by 25 RF cycles (2.5 μs). The images show that while there are rapid variations in the electron density, there are features that persist over many RF cycles. A limited range of values (0.9–1.35 $\times$ 10^{10} cm^{-3}) is plotted to emphasize the filaments. Contour labels are multipliers of 10^{10} cm^{-3}.

Filaments in the electron density and excited state densities were a natural outcome of the multifluid, collisional plasma hydrodynamics model used in the investigation while employing tensor transport coefficients and mildly anomalous cross field diffusion. At a pressure of 40 mTorr, the onset of filamentation occurred at a magnetic field of about $B_z = 500$ G. Experimentally, the filaments are observed by visible optical emission, which in the model is represented by the density of excited states, here being the Ar(4p) manifold. Filamentation also occurred in the electron temperature and in the plasma potential, but was most severe for optical emission. This more severe filamentation is due to the short lifetime of the excited states, which are more sensitive to small variations in electron temperature (electron impact rate coefficients) and electron density. The filaments were mobile, moving parallel to the electrodes, while colliding, merging, and separating.

Several computational experiments were performed (e.g., varying pressure, gap separation, and secondary emission coefficient) to determine the source of the filaments. The strongest correlation was with the conductivity of the plasma facing surface opposite the powered electrode. When the top surface was metal, the filaments did not occur. When the top surface was dielectric with negligible conductivity, filaments did occur. As the surface conductivity of the plasma facing dielectric was artificially increased, the filaments dissipated. When then examining the surface charge on the dielectric, there are maximum and minima in the surface charge that correlate with the filaments. The interpretation is as follows.

For sufficiently large magnetic fields, charge transport in the plasma is dominantly along the field lines, terminating on the dielectric surface. The surface charges and discharges during the RF cycle while remaining negative, in an attempt to maintain the floating potential with respect to the adjacent plasma. Since the plasma is not uniform in the lateral direction (that is, electron and ion temperatures, plasma density, and plasma potential laterally vary), the natural charging of the dielectric is also not uniform even in the absence of a magnetic field. However, the charging is smooth. With a magnetic field, the stringent balance of fluxes on any given magnetic field line connecting to its underlying surface charge can be perturbed by its neighbor, which then leads to more (or less) surface charging to attempt to balance fluxes. If there is, for example, overshoot in favor of an excess of negative surface charge, the plasma density on the adjacent magnetic field line increases. If there is an undershoot producing a deficit of negative surface charge, the electron density on the adjacent field line decreases. The correlation with plasma potential on the magnetic field line is less clear. The plasma potential naturally oscillates in response to the applied potential and to reverse the direction of the applied electric field. The increase in the electron density on a field line in response to the surface charging produces a phase dependent perturbation in plasma potential. Once the surface charge under a single magnetic field line is perturbed, the perturbation is transmitted from one field line to another.

The lack of filamentation with a metal electrode is due to the lack of surface charging to perturb adjacent flux ropes. Increasing the sheet conductivity on an otherwise dielectric electrode enables more rapid balancing of the perturbed surface charge than is possible by cross field transport in the bulk plasma. This increasing sheet conductivity also

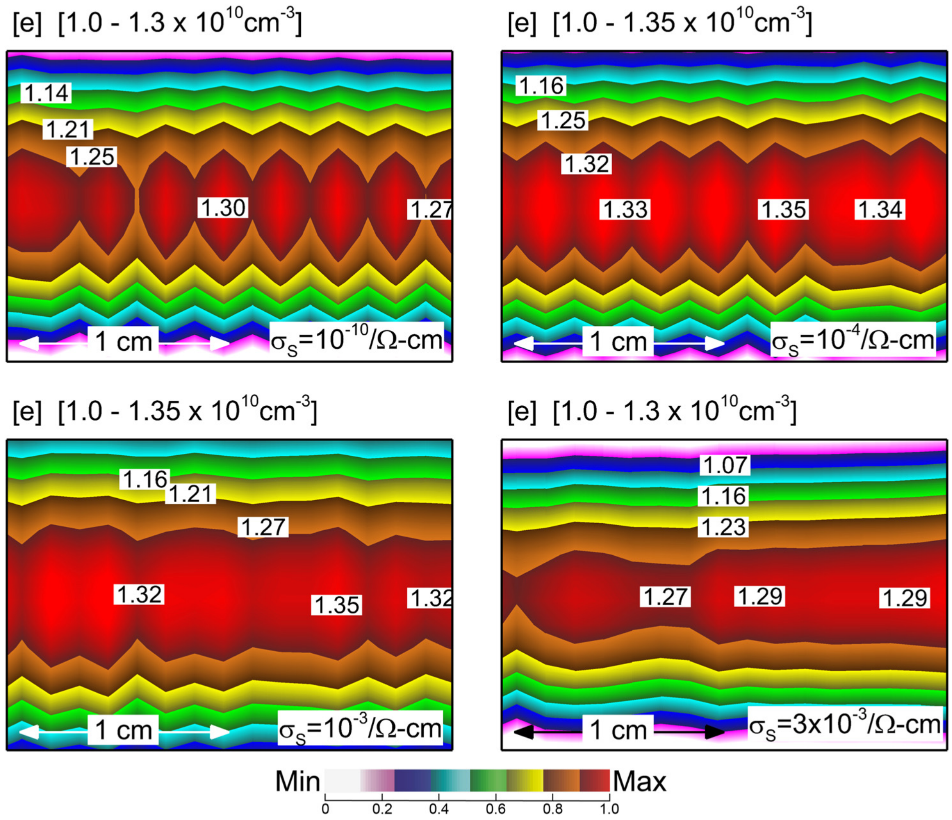

FIG. 7. Electron densities at the midgap (the same location as in Figs. 4 and 5) for $B_z = 3500$ G as a function of the surface or sheet conductivity of the plasma facing dielectric. The default conductivity of the dielectric is $\sigma = 10^{-10}/\Omega$ cm. Increasing the sheet conductivity to $\sigma_S = 10^{-5}/\Omega$ cm had little effect on the filaments. As σ_S increased to $10^{-4}/\Omega$ cm and higher, the filaments began to dissipate. Limited ranges of values (indicated in each image) are plotted to emphasize the filaments. Contour labels are multipliers of 10^{10} cm^{-3}.

enables the charge density (positive and negative) trapped on magnetic field lines to communicate through the conductivity of the surface and negate those charge differences. A particularly large rate of anomalous cross field electron transport would accomplish the same ends of negating disparate charge that produces the filaments.

This conclusion from the simulation results is particularly interesting because of its implication for dusty plasma experiments. First, it would suggest that a new, dedicated experimental study that is focused on characterizing the formation of filaments in a pristine metal-on-metal vs metal-on-dielectric electrode—possibly having both configurations simultaneously—could provide an important test and validation of the simulation results in the absence of dust particles. Second, in many of these experiments, as the dust particles are shaken into the experimental volume, a layer of dust particles is built up on the surfaces of the electrodes. In most experiments, these dust particles are alumina, silica, or melamine-formaldehyde—which are all dielectric materials. These simulation results would suggest that the presence of the dielectric layer of the dust particles themselves may be partially responsible for the presence of the filaments.

ACKNOWLEDGMENTS

This work was supported by the U.S. Department of Energy (DOE), Office of Fusion Energy Sciences Program and the U.S. National Science Foundation (NSF). Computational efforts were supported by DOE Grant Nos. DE-SC0001939 and DE-SC0014132 and NSF Grant No. PHY-1500126. The experimental results presented in this paper were based upon the work supported by DOE Grant No. DE-SC0016330 and by NSF Grant No. PHY-1613087. The construction of the MDPX device was funded through the NSF Major Research Instrumentation program, Grant No. PHY-1126067. Additional support was provided by the NSF EPSCoR program (No. OIA-1655280). Special thanks to Stephen Williams at Auburn University who provided the images of the filaments from the experiments on the MDPX device.

REFERENCES

[1] A. Piel and A. Melzer, "Dusty plasmas-the state of understanding from an experimentalist's view," Adv. Space Res. **29**, 1255 (2002).
[2] A. Piel and A. Melzer, "Dynamical processes in complex plasmas," Plasma Phys. Controlled Fusion **44**, R1 (2002).
[3] P. K. Shukla, "A survey of dusty plasma physics," Phys. Plasmas **8**, 1791 (2001).
[4] R. L. Merlino and J. Goree, "Dusty plasmas in the laboratory, industry, and space," Phys. Today **57**(7), 32 (2004).
[5] A. Barkan, N. D'Angelo, and R. Merlino, "Charging of dust grains in a plasma," Phys. Rev. Lett. **73**, 3093 (1994).
[6] B. Walch, M. Horanyi, and S. Robertson, "Measurement of the charging of individual dust grains in a plasma," IEEE Trans. Plasma Sci. **22**, 97 (1994).
[7] E. Thomas and M. Watson, "Charging of silica particles in an argon dusty plasma," Phys. Plasmas **7**, 3194 (2000).
[8] H. Ikezi, "Coulomb solid of small particles in plasmas," Phys. Fluids **29**, 1764 (1986).
[9] A. Melzer, A. Homann, and A. Piel, "Experimental investigation of the melting transition of the plasma crystal," Phys. Rev. E **53**, 2757 (1996).
[10] R. A. Quinn and J. Goree, "Experimental investigation of particle heating in a strongly coupled dusty plasma," Phys. Plasmas **7**, 3904 (2000).

[11] O. Vaulina, I. Drangevski, and X. Adamovich, "Two-stage melting in quasi-two-dimensional dissipative Yukawa systems," Phys. Rev. Lett. **97**, 195001 (2006).

[12] V. Nosenko, S. Zhdanov, A. Ivlev, G. Morfill, J. Goree, and A. Piel, "Heat transport in a two-dimensional complex (dusty) plasma at melting conditions," Phys. Rev. Lett. **100**, 25003 (2008).

[13] D. Samsonov, A. V. Ivlev, R. A. Quinn, G. Morfill, and S. Zhdanov, "Dissipative longitudinal solitons in a two-dimensional strongly coupled complex (dusty) plasma," Phys. Rev. Lett. **88**, 095004 (2002).

[14] T. E. Sheridan, V. Nosenko, and J. Goree, "Experimental study of nonlinear solitary waves in two-dimensional dusty plasma," Phys. Plasmas **15**, 073703 (2008).

[15] J. H. Chu and I. Lin, "Direct observation of Coulomb crystals and liquids in strongly coupled rf dusty plasmas," Phys. Rev. Lett. **72**, 4009 (1994).

[16] H. Thomas, G. Morfill, V. Demmel, J. Goree, B. Feuerbacher, and D. Möhlmann, "Plasma crystal: Coulomb crystallization in a dusty plasma," Phys. Rev. Lett. **73**, 652 (1994).

[17] Y. Hayashi and K. Tachibana, "Observation of Coulomb-crystal formation from carbon particles grown in a methane plasma," Jpn. J. Appl. Phys., Part 2 **33**, L804 (1994).

[18] U. Konopka, M. Schwabe, C. Knapek, M. Kretschmer, and G. E. Morfill, "Complex plasmas in strong magnetic field environments," AIP Conf. Proc. **799**, 181 (2005).

[19] M. Schwabe, U. Konopka, P. Bandyopadhyay, and G. E. Morfill, "Pattern formation in a complex plasma in high magnetic fields," Phys. Rev. Lett. **106**, 215004 (2011).

[20] E. Thomas, Jr., U. Konopka, R. L. Merlino, and M. Rosenberg, "Initial measurements of two- and three-dimensional ordering, waves, and plasma filamentation in the magnetized dusty plasma experiment," Phys. Plasmas **23**, 055701 (2016).

[21] M. Schwabe, "Microparticles as probes in a highly magnetized dusty plasma," Diploma of Physics thesis, Technical University of Munich (TUM), 2006.

[22] E. Thomas, Jr., R. L. Merlino, and M. Rosenberg, "Magnetized dusty plasmas: The next frontier for complex plasma research," Plasma Phys. Controlled Fusion **54**, 124034 (2012).

[23] E. Thomas, U. Konopka, D. Artis, B. Lynch, S. LeBlanc, S. Adams, R. L. Merlino, and M. Rosenberg, "The magnetized dusty plasma experiment (MDPX)," J. Plasma Phys. **81**, 345810206 (2015).

[24] A. Hecimovic and A. von Keudell, "Spokes in high power magnetron sputtering plasmas," J. Phys. D: Appl. Phys. **51**, 453001 (2018).

[25] R. Kawashima, K. Hara, and K. Komurasaki, "Numerical analysis of azimuthal rotating spokes in a cross-field discharge plasma," Plasma Sources Sci. Technol. **27**, 035010 (2018).

[26] M. J. Kushner, "Hybrid modelling of low temperature plasmas for fundamental investigations and equipment design," J. Phys. D: Appl. Phys. **42**, 194013 (2009).

[27] S. H. Song, Y. Yang, P. Chabert, and M. J. Kushner, "Electron energy distributions in a magnetized inductively coupled plasma," Phys. Plasmas **21**, 093512 (2014).

[28] M. J. Grapperhaus, Z. Krivokapic, and M. J. Kushner, "Design issues in ionized metal physical vapor deposition of copper," J. Appl. Phys. **83**, 35 (1998).

[29] M. J. Kushner, "Modeling of magnetically enhanced capacitively coupled plasma sources: Ar discharges," J. Appl. Phys. **94**, 1436 (2003).

[30] P. Tian and M. J. Kushner, "Controlling VUV photon fluxes in low-pressure inductively coupled plasmas," Plasma Sources Sci. Technol. **24**, 034017 (2015).

[31] T. Hall, E. Thomas, Jr., K. Avinash, R. Merlino, and M. Rosenberg, "Methods for the characterization of imposed, ordered structures in MDPX," Phys. Plasmas **25**, 103702 (2018).

[32] R. J. Powell and M. Morad, "Optical absorption and photoconductivity in thermally grown SiO_2 films," J. Appl. Phys. **49**, 2499 (1978).

[33] J. L. Lauer, J. L. Shohet, C. Cismaru, R. W. Hansen, M. Y. Foo, and T. J. Henn, "Photoemission and conduction currents in vacuum ultraviolet irradiated aluminum oxide," J. Appl. Phys. **91**, 1242 (2002).